Occurrences of high-K calc-alkaline shoshonitic granitoids in the Northeastern part of Shillong Plateau, Meghalaya, India

M. Faruque Hussain* and Debjani Choudhury

Department of Earth Science, Assam University, Silchar 788 011, India

Shoshonitic rocks represent the transition between calc-alkaline and alkaline rocks, often formed during the last stages of uplift in zones of continental collision. This study describes the characterization of Kyrdem granitoids of Shillong plateau, Meghalaya, North East India, as felsic shoshonites. The study also documents petrogenesis of the shoshonites and suggests significant magma mixing and crust–mantle melt interaction as prime mechanisms for parental magma evolution. Crustal melt has most probably been sourced from a metabasaltic middle crust, while the mantle source is represented by an enriched sub-continental lithospheric mantle, metasomatized by sediment melt, during an earlier subduction event.

Keywords: Calc-alkaline rocks, continental collision, felsic shoshonites, geochemistry, magma evolution.

CALC-ALKALINE to shoshonitic rocks are widely distributed in many orogenic belts[1,2], often formed during the last stages of uplift in zones of continental collision[3]. Some workers have suggested that such rock associations are related to subduction processes[4], while others have argued that they generally form in post-collisional extensional settings[5]. Petrogenetic studies revealed they could have been derived from a subcontinental lithospheric mantle or metasomatized sub-arc mantle, like the Pliocene mafic potassic rocks of the Sierra Nevada[6] and volcanism in the north Mariana arc[7]. They could have also originated from the asthenospheric mantle, as indicated by the Early Cretaceous potassium-rich basalts in Inner Mongolia[8]. Shoshonitic rocks can also be formed by joint contributions from crust–mantle interactions[9]. In addition to the source(s), magma differentiation processes, such as fractional crystallization, magma mixing and crustal contamination, also play a significant role in the genesis of both shoshonites and associated calc-alkaline rocks[1].

Geology of Shillong plateau

The present study reports the occurrence of shoshonitic magmatic rocks from the Kyrdem Pluton in the Shillong Plateau, Meghalaya, North East India. The Shillong Plateau predominantly comprises an assembly of Paleoproterozoic basement terrain intruded by multiple phases of felsic and mafic magmatic rocks underlain by Mesoproterozoic Shillong Group of supracrustals and overlain by Tertiary sediments. The Plateau is bounded by the Dauki Fault in the south, the Brahmaputra Fault in the north and the Jamuna Fault in the west (Figure 1 *a*). The Kopili rift in the east separates the Shillong Plateau from the Mikir Hills, which represent the eastern extension of the Plateau (Figure 1 *a*). The basement assembly is composed of amphibolite to granulite facies gneisses, mafic granulites, migmatites, metapelitic granulites and quartzo-feldspathic gneisses[10]. The Shillong Group of rocks is represented by a thick pile of quartzites and phyllites. The basement assembly of the Shillong Plateau was intruded by three distinctly identifiable episodes of magmatic activities. The earliest episode was of basaltic magmatism during Mesoproterozoic, presently represented by meta-dolerites (locally known as Khasi Greenstones), followed by an episode of granitoid plutonism (430–535 Ma)[11] represented by South Khasi, Mylliem, Nongpoh and Kyrdem plutons. The last episode is marked by Sylhet Trap volcanism (117 Ma)[12] and associated ultramafic–alkaline–carbonatite (UAC) magmatism[13]. Tertiary sediments flank the plateau along its periphery, with thicker piles of sediment occurring in the east and southwest (Figure 1 *a*).

Petrography

In the north–central part of Shillong Plateau, Kyrdem granitoids have been emplaced, which occurs predominantly within 92–92°10′E long. and 25°38′–25°50′N lat. (Figure 1 *b*). It comprises coarse-grained, grey- and pink-coloured porphyritic granitoids with abundant feldspar phenocrysts (up to 6 cm long) (Figure 2 *a*) and inclusions of microgranular mafic enclaves (Figure 2 *b*). The enclaves are variable in size, ranging from a few centimetres up to a few metres across or more, and typically have either sharp or reactive contacts with the host granitoids.

Petrographically the granitoids range in composition from syenogranites to monzogranites. These are composed of K-feldspar (27–37 vol%), plagioclase (26–32 vol%),

*For correspondence. (e-mail: faruque.esc@gmail.com)

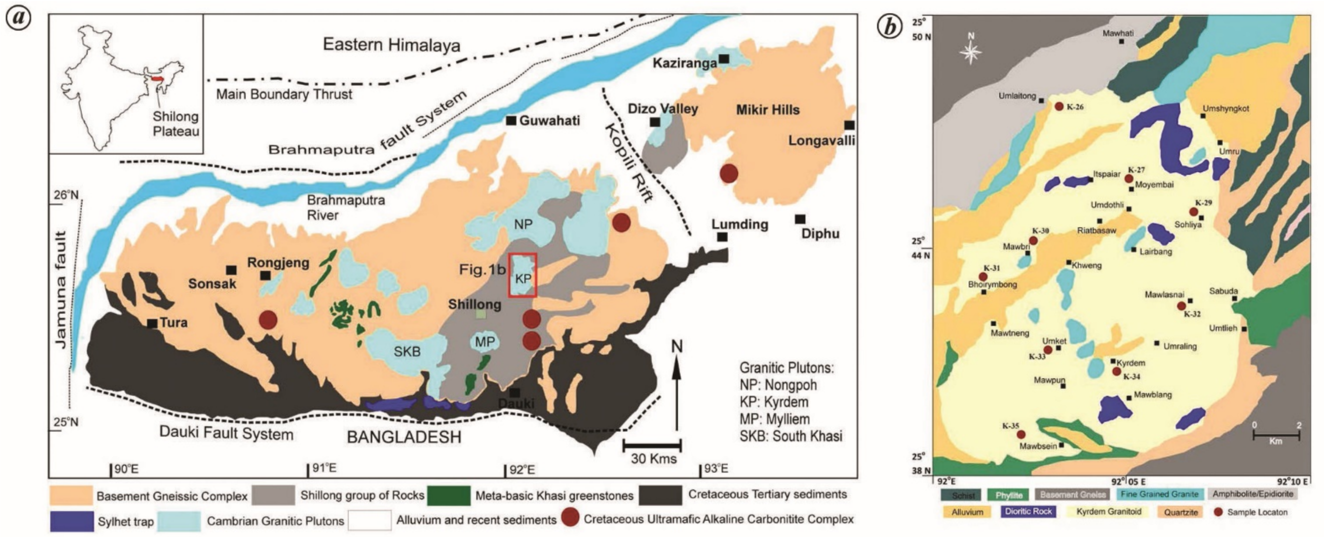

Figure 1. ***a***, Regional and geological map of the Shillong Plateau, Meghalaya, North East India[47]. ***b***, Geological map of the area around Kyrdem Pluton, Shillong Plateau (modified after Kumar and Singh[48]).

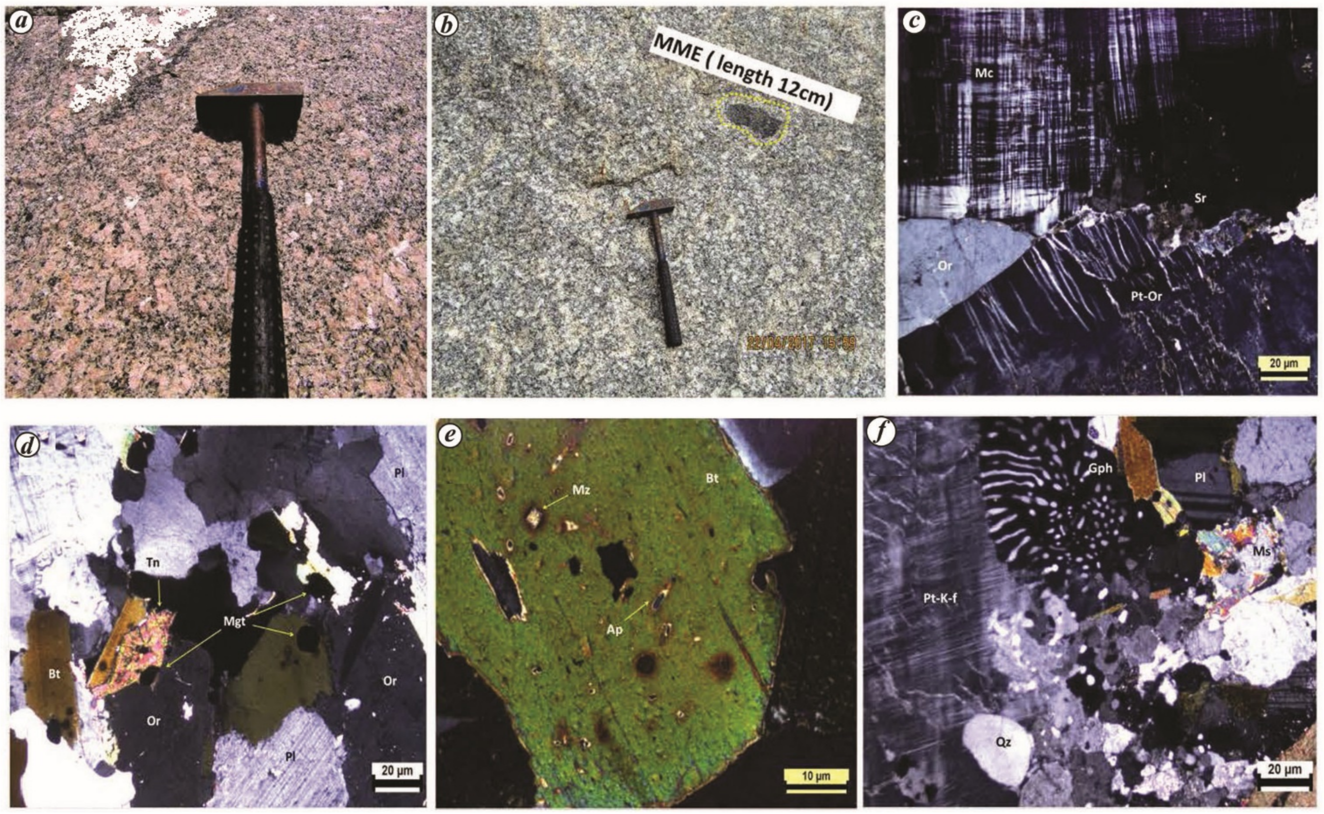

Figure 2. Field photographs and photomicrographs of the Kyrdem granitoid samples showing (***a***) pink porphyritic K-feldspar (K-f) grains; (***b***) inclusions of microgranular mafic enclaves (MMEs); (***c***) orthoclase (Or) grain with exsolved perthitic blebs (Pt–Or) and flames, and microcline grain with cross-hatched twinning both being sericitized (Sr) along the contact zone; (***d***) Or grains with microperthites, plagioclase showing albite twining, partly altered titanite (Tn) grains and biotites with the release of magnetite (Mgt); (***e***) presence of accessories like apatite (Ap) and monazite (Mz) within the euhedral biotite grains and (***f***) perthitic microcline (Pt–K–f), plagioclase, graphic texture (Gph) and quartz droplets which are by-products of alteration reactions and muscovitization (Ms).

quartz (32–45 vol%), biotite (8–10 vol%), hornblende (5–8 vol%) and minor pyroxenes. K-feldspars are generally microclines (perthitic) which occur as phenocrysts and are conspicuously large-sized (Figure 2 *c*). Sphene, zircon, apatite, monazite, ilmenite and magnetite are the common accessories within biotites (Figure 2 *d* and *e*). Graphic and

Table 1. Major oxides analysis (wt%), Cross, Iddings, Pirsson and Washington (CIPW) normative compositions (wt%) and important major oxide parameters of the Kyrdem granitoids in Shillong Plateau, Meghalaya, North East India

Sample no.	K-26	K-27	K-29	K-30	K-31	K-32	K-33	K-34	K-35	Avg
Major oxides (wt%)										
SiO_2	65.2	64.8	65.7	67.9	67.4	66.0	66.2	65.2	66.2	66.1
TiO_2	0.91	0.80	0.81	0.63	0.63	0.75	0.64	0.72	0.68	0.73
Al_2O_3	14.9	15.2	14.6	14.7	14.9	14.9	15.3	15.3	15.0	15.0
MnO	0.09	0.08	0.09	0.06	0.06	0.08	0.06	0.07	0.07	0.07
$Fe_2O_3^T$	5.17	4.88	4.92	3.70	3.72	4.42	3.95	4.46	4.24	4.88
CaO	3.57	3.53	3.58	2.91	2.97	2.96	2.91	3.15	2.91	3.17
MgO	2.09	1.85	1.83	1.40	1.40	1.78	1.54	1.73	1.58	1.69
Na_2O	2.64	2.63	2.61	2.46	2.49	2.44	2.47	2.54	2.42	2.52
K_2O	4.35	4.94	4.45	5.19	5.19	5.46	5.79	5.48	5.59	5.16
P_2O_5	0.45	0.45	0.43	0.33	0.33	0.41	0.38	0.40	0.40	0.40
Total	99.37	99.17	99.06	99.27	99.09	99.16	99.27	99.08	99.12	99.18
LOI	0.60	0.418	0.601	0.427	0.390	0.423	0.412	0.392	0.388	
Na_2O/K_2O	0.61	0.53	0.59	0.47	0.48	0.45	0.43	0.46	0.43	0.49
A/CNK	0.96	0.94	0.94	0.98	0.98	0.97	0.98	0.97	0.98	0.97
A/NK	1.64	1.57	1.61	1.52	1.53	1.50	1.48	1.52	1.49	1.54
FeO^T/MgO	2.23	2.37	2.42	2.38	2.39	2.23	2.31	2.32	2.41	2.34
$Fe_2O_3^T + MnO + MgO$	7.35	6.81	6.84	5.16	5.18	6.28	5.55	6.26	5.89	6.15
$Na_2O + K_2O$	6.99	7.57	7.06	7.65	7.68	7.9	8.26	8.02	8.01	7.68
R1	2239	2087	2264	2327	2264	2121	2067	2028	2124	2028
R2	777	767	761	669	679	697	687	724	683	723
Mg#	31	29.6	29.2	29.6	29.5	30.9	30.2	30.1	29.3	29.9
CIPW norms (wt%)										
Quartz	23.8	20.1	24.3	26.4	25.6	23.0	22.3	21.2	23.3	23.3
Albite	22.3	22.3	22.1	20.8	21.2	20.7	21.0	21.5	20.5	21.3
Anorthite	14.8	13.7	15.0	12.3	12.6	12.0	12.0	13.0	11.8	13.0
Orthoclase	25.7	31.8	26.3	30.7	30.7	32.3	34.2	32.4	33.0	30.8
Corundum	0.38	0.00	0.05	0.52	0.56	0.57	0.55	0.45	0.59	0.41
Sphene	0.00	0.62	0.00	0.00	0.00	0.00	0.00	0.00	0.00	0.07
Hypersthene	5.21	4.61	4.56	3.49	3.49	4.43	3.84	4.31	3.94	4.21
Rutile	0.81	0.46	0.71	0.56	0.56	0.66	0.57	0.64	0.60	0.62
Ilmenite	0.19	0.17	0.19	0.13	0.13	0.17	0.13	0.15	0.15	0.16
Hematite	5.17	4.88	4.92	3.70	3.72	4.42	3.95	4.46	4.24	4.38
Apatite	1.08	1.04	1.00	0.76	0.76	0.95	0.88	0.93	0.93	0.92
Total	99.4	99.6	99.1	99.3	99.1	99.2	99.3	99.1	99.1	99.2

A/NK = Molar $Al_2O_3/(Na_2O + K_2O)$; A/CNK = Molar $Al_2O_3/(CaO + Na_2O + K_2O)$; $FeO^T = Fe_2O_3^T$ (wt%)/0.8998; Mg# = 100 × MgO/(MgO + FeO); R1 = 4Si-11(Na + K)-2(Fe + Ti) and R2 = 6Ca + 2Mg + Al. All the elements are expressed in terms of millications.

myrmekitic intergrowth of quartz and plagioclase is also common (Figure 2 *f*).

Geochemistry analytical techniques

Nine granitoid samples were analysed for major oxides at the National Centre of Earth Science Studies (NCESS), Thiruvananthapuram, Kerala, India, using WD-XRF (Bruker S4 Pioneer sequential wavelength-dispersive X-ray spectrometer, Bruker, Germany) and trace elements, including rare earth elements (REE) at the CSIR-National Geophysical Research Institute (CSIR-NGRI), Hyderabad, using HR-ICP-MS (Nu Instruments, Attom, UK). Certified international references G-2 and JG-1a were used as standards. Analytical procedures for X-ray fluorescence (XRF) analyses were according to Kumar and Sreejith[14]. The precision and accuracy for XRF analyses were found to be better than 3% and 5% respectively. For REE analysis, sample preparation was carried out following the closed digestion technique. The detection limits for most trace elements, including REEs, were around 0.01 ng/ml, and precision was better than 6% RSD for trace elements and REEs. The analysed data of the granitoids are presented in Tables 1 and 2, along with Cross, Iddings, Pirsson and Washington (CIPW) norms and important major and trace element ratios.

Major, trace and rare earth elements (REE) geochemistry

The studied granitoids have SiO_2 content between 65.19 and 67.91 wt%, and K_2O content between 4.35 and 5.79 wt%, comparable to shoshonitic granitoids from other sources (e.g. East Junggar, NW China[5]; Raghunathpur granitoid batholith, eastern India[9]; western Tianshan orogen and central Asian orogenic belt[15]). The Na_2O (2.42 to 2.64 wt%), CaO (2.91 to 3.58 wt%), MgO (1.40 to 2.09 wt%), Al_2O_3

Table 2. Trace and rare earth element (REE) data and few important ratios of trace and REE of the Kyrdem granitoids in Shillong Plateau

Sample no.	K-26	K-27	K-29	K-30	K-31	K-32	K-33	K-34	K-35	Avg
Trace elements (ppm)										
Sc	13	11	17	9	9	12	9	10	10	11
V	81	74	76	55	56	74	60	72	66	68
Cr	109	91	101	102	106	106	86	95	96	99
Co	13	11	11	9	9	11	9	11	10	10
Ni	9	6	6	6	6	9	6	7	6	7
Cu	3	2	2	2	2	2	2	2	2	2
Zn	34	11	13	28	19	22	21	13	17	20
Ga	24	24	23	21	21	24	21	24	22	23
Rb	203	233	209	210	208	252	230	247	238	225
Sr	480	506	494	501	499	542	518	540	514	510
Y	92	71	81	57	56	79	59	70	62	70
Zr	360	363	288	193	198	225	220	275	247	263
Nb	40	36	39	28	27	40	28	34	30	33
Cs	6	5	5	4	4	5	4	5	5	5
Ba	1348	1317	1348	1534	1447	1615.2	1691	1507	1665	1497
Hf	11	11	9	6	6	7	7	8	8	8
Ta	3	4	6	2	2	2	2	3	3	3
Pb	37	41	40	42	42	46	45	44	45	43
Th	32	44	45	42	38	39	36	52	45	42
U	6	9	8	7	7	9	7	9	8	8
REEs (ppm)										
La	99.2	112	129	118	101	113	98.2	112	114	111
Ce	233	235	260	233	206	235	199	230	227	229
Pr	31.5	32.1	34.6	30.6	27.4	32.2	26.9	30.9	30.3	30.7
Nd	108	107	112	97.9	89.6	107	89.7	101	99.2	10
Sm	22.5	20.4	21.1	17.5	16.5	21.2	17.2	19.3	18.4	19.3
Eu	3.52	3.10	3.29	2.68	2.60	3.41	2.87	3.06	2.98	3.06
Gd	15.5	13.1	14.1	11.2	10.6	13.9	11.3	12.6	12.1	12.7
Tb	2.88	2.33	2.52	1.96	1.87	2.54	2.00	2.24	2.12	2.27
Dy	13.5	10.5	11.5	8.75	8.45	11.7	9.07	10.1	9.48	10.3
Ho	2.34	1.81	2.01	1.48	1.44	1.98	1.55	1.73	1.60	1.77
Er	7.00	5.35	6.09	4.37	4.24	5.98	4.54	5.14	4.68	5.27
Tm	1.13	0.85	0.97	0.68	0.66	0.96	0.70	0.80	0.73	0.83
Yb	7.84	5.68	6.64	4.56	4.49	6.59	4.67	5.49	4.95	5.66
Lu	1.22	0.88	1.06	0.70	0.68	1.02	0.71	0.86	0.76	0.88
∑LREE	514	523	575	512	454	528	445	511	504	507
∑HREE	35.9	27.4	30.8	22.5	21.8	30.7	23.2	26.4	24.3	27.0
∑REE	550	550	606	534	476	558	468	537	529	534
Zr + Nb + Ce + Y	726	705	669	512	488	580	507	609	566	596
Eu/Eu*	0.58	0.58	0.58	0.59	0.60	0.61	0.63	0.60	0.61	0.60
La/Sm	4.42	5.50	6.14	6.81	6.15	5.38	5.70	5.86	6.19	5.79
Sm/Nd	0.21	0.19	0.19	0.18	0.18	0.20	0.19	0.19	0.19	0.19
Ce/Nd	2.14	2.20	2.31	2.38	2.31	2.19	2.22	2.27	2.29	2.26
Ce/Yb	29.8	41.4	39.3	51.2	46.1	35.8	42.7	42.0	46.0	41.6
Ta/Yb	0.34	0.63	0.86	0.47	0.42	0.34	0.42	0.50	0.56	0.50

(14.64 to 15.33 wt%) and $Fe_2O_3^T$ (3.70 to 5.17 wt%) rock contents were also similar to those of shoshonites. A list of granitoids from different plutons of the Shillong Plateau and Chhotanagpur gneissic complex are presented in Table 3 along with the studied Kyrdem granitoids to compare in their major element geochemistry, nature, tectonic setting and age. The studied rocks were characterized by the presence of corundum, hypersthene, rutile, ilmenite, hematite and apatite in the norms. They showed quartz–monzonite and monzogranite affinity (Ab–An–Or plot; Figure 3 *a*), were metaluminous (A/NK: 1.48–1.64, A/CNK: 0.94–0.98) and fell within the field of magnesian post-Caledonian granitoid plutons (Figure 3 *b*). However, in the K_2O versus SiO_2; Na_2O versus K_2O; Ce/Yb versus Ta/Yb and Th/Yb versus Ta/Yb plots (Figures 3 *c–f*), they display shoshonitic affinity. Shoshonitic rocks with $SiO_2 > 63$ wt% are known as felsic shoshonites[16] or shoshonitc granitoids[9]. The distinctive parameters for shoshonitic granitoids such as high alkali content ($K_2O + Na_2O > 5$ wt%)[17], low TiO_2 content (<1.2 wt%)[16], high K_2O and P_2O_5 contents and high K_2O/Na_2O (>0.8) and SiO_2/P_2O_5 ratios[9,18–20] corresponded well with the granitoid samples. They were characterized by high abundances of large-ion lithophile elements (LILEs) like Sr (480–543 ppm: avg = 510 ppm), Ba

Table 3. Comparison of geochemical characteristics and tectonic setting of the granitoids of Kyrdem pluton with rocks of other felsic plutons of the Shillong Plateau and Chhotanagpur Plateau

Plutons	Rock type	(A/CNK versus A/NK)	MALI versus SiO_2	Nature	Tectonic setting	Age (Ma)
Kyrdem	Monzogranite	Metaluminous	Calc-alkalic, alkali calcic	Shoshonitic granitoids	Post-collisional tectonic regime	512.5 ± 8.7
Mylliem	Monzogranite–syenogranite	Mildly peraluminous	Calc-alkalic, alkali calcic, alkalic	I-type		508.2 ± 8.6
Nongpoh	Quartz–monzonite	Metaluminous				506 ± 7.1
Kyllang	Granite, granodiorite, quartz–monzonite	Peraluminous	Alkalic	Calc-alkaline S-type	Within plate collisional phase in subduction environment	510.6 ± 7.6
Sindhuli	Granite, quartz–monzonite	Metaluminous–peraluminous		Calc-alkaline I-type	Post-collisional	881 ± 39
Rongjeng	Monzogranite	Peraluminous	Calc-alkalic	S-type	Volcanic arc setting	788 ± 22
Kaziranga	Monzogranite	Peraluminous	Alkalic	S-type	Within-plate to syn-collisional	528.7 ± 5.5
Raghunathpur granitoids, Chhotanagpur Gneissic Complex	Granite, granodiorite, tonalite, quartz–syenite and quartz–monzonite	Metaluminous–peraluminous	Calc-alkalic, alkali calcic, alkalic	Shoshonitic granitoids	Post-collisional	1071 ± 64
Jhalida granitoids, Chhotanagpur Gneissic Complex	Syenogranite, monzogranite and granodiorite	Metaluminous to weakly peraluminous	Calc-alkalic, alkali calcic, alkalic	Shoshonitic granitoids	Post-collisional	–

Data for the granitoids of Kyrdem, Mylliem, Nongpoh, Rongjeng and Kaziranga plutons are from Kumar *et al.*[11]; Kyllang pluton from Singh[44]; Sindhuli pluton from Ghosh *et al.*[50]; Raghunathpur granitoids from Goswami and Bhattacharyya[9] and Jhalida granitoids from Roy *et al.*[35].

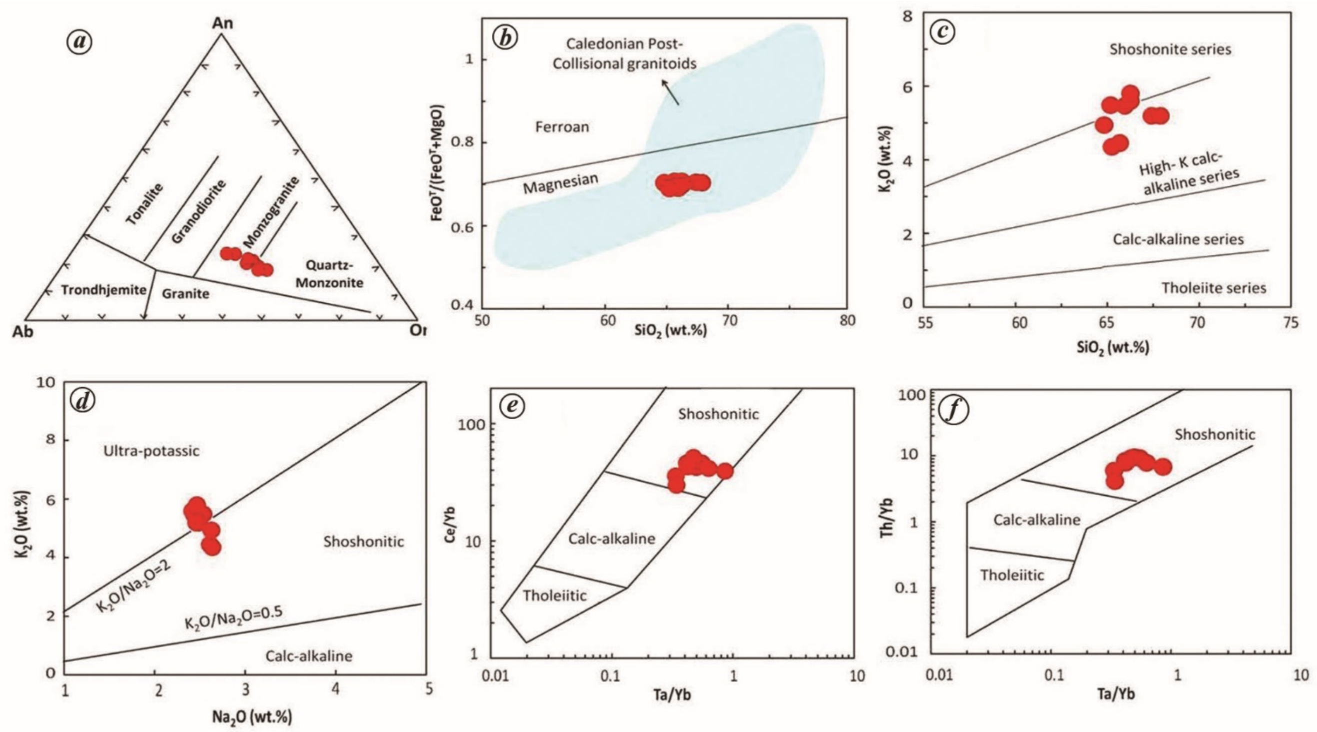

Figure 3. ***a***, Ab–An–Or plot[51,52]; ***b***, Fe-number [$FeO^T/(FeO^T + MgO)$] versus SiO_2 plot[53]; ***c***, K_2O versus SiO_2 variation diagram[54]; ***d***, K_2O versus Na_2O diagram[17]; ***e***, Ta/Yb versus Ce/Yb[55]; ***f***, Ta/Yb versus Th/Yb plot[55] for the Kyrdem granitoids.

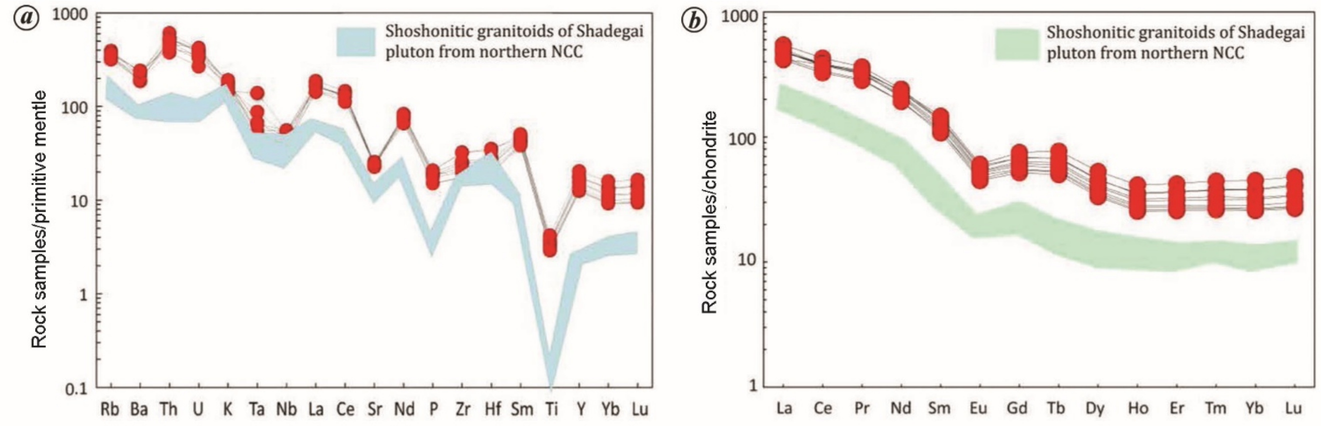

Figure 4. ***a***, PM-normalized multi-elemental plot. ***b***, Chondrite normalized rare earth elements plot of Kyrdem granitoids. (The normalizing values are after Sun and McDonough[22], with the field of shoshonitic granitoids from northern North China Craton after Jia *et al.*[20].)

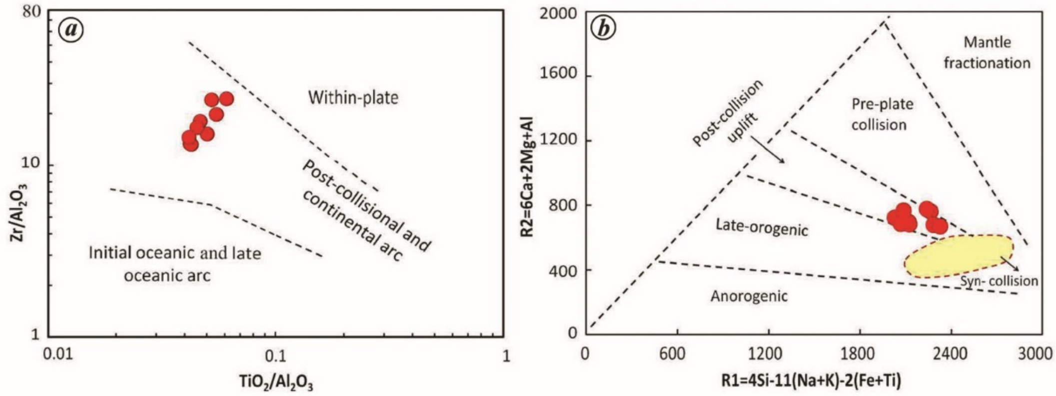

Figure 5. Tectonic discrimination plots for the Kyrdem granitoids: (***a***) TiO_2/Al_2O_3 versus Zr/Al_2O_3 plot[24] and (***b***) R1–R2 multi-cationic diagram[25,26].

(1316–1691 ppm: avg = 1497 ppm), Pb (37–46 ppm: avg = 43 ppm), Th (32–52 ppm: avg = 42 ppm), U (6–9 ppm: avg = 8 ppm) and Rb (203–252 ppm: avg = 226 ppm), similar to shoshonites. The concentration of high field-strength elements (HFSEs) in Kyrdem granitoids (KG) like Zr (193–364 ppm: avg = 264 ppm), Ta (2–6 ppm: avg = 3 ppm), Hf (6–11 ppm: avg = 8), Y (57–92 ppm: avg = 70 ppm) and Nb (27–40 ppm: avg = 30 ppm) was also within the limits of felsic shoshonites (Table 2). Furthermore, the Zr/Hf ratio between 32.07 and 34.04, was consistent with shoshonitic igneous rocks[21].

The primitive mantle (PM) normalized (normalizing values[22]) multi-element patterns for the samples showed parallel and enriched trends with enrichment of LILE (60–700 times PM) compared to HFSE (8–30 times PM), which also supports their typical shoshonitic nature (Figure 4 *a*). The studied samples displayed identical chondrite-normalized REE patterns, with significant enrichment in LREEs (400–600 times the chondrite value), depletion in HREE (25–50 times of chondrite value) and weakly negative Eu anomalies (Figure 4 *b*). Based on the above petrological and geochemical characteristics, the granitoids of Kyrdem pluton have been distinguished as felsic shoshonites[23].

Occurrences of magmatic rocks with shoshonitic affinity from extensional or post-collisional settings are not uncommon[3,9,19,20]. The studied granitoids with strong enrichment of incompatible elements (LILE and LREE) and significant negative Nb, Zr and Ti anomalies (Figure 4 *a*) suggest subduction and post-collisional settings[20]. In the TiO_2/Al_2O_3 versus Zr/Al_2O_3 plot[24], proposed for tectonic discrimination of potassic and ultrapotasic rocks, the Kyrdem granitoid samples occurred conspicuously within the fields of post-collisional and continental arc magmas (Figure 5 *a*). In the R1–R2 multi-cationic plot[25,26], most of the studied samples fell in the boundary between the orogenic group and the post-collision uplift granite group (Figure 5 *b*).

Discussion

The high SiO_2 (avg: 66.1 wt%) and low MgO (avg: 1.69 wt%) contents, along with low ratios of Nb/La (avg: 0.30) and Zr/Hf (avg: 32.7), suggest the addition of crustal melt to the magma source of the granitoids[27]. In addition, there are field evidences of the basic and felsic magma interactions (e.g. presence of mafic enclaves) within the plutonic

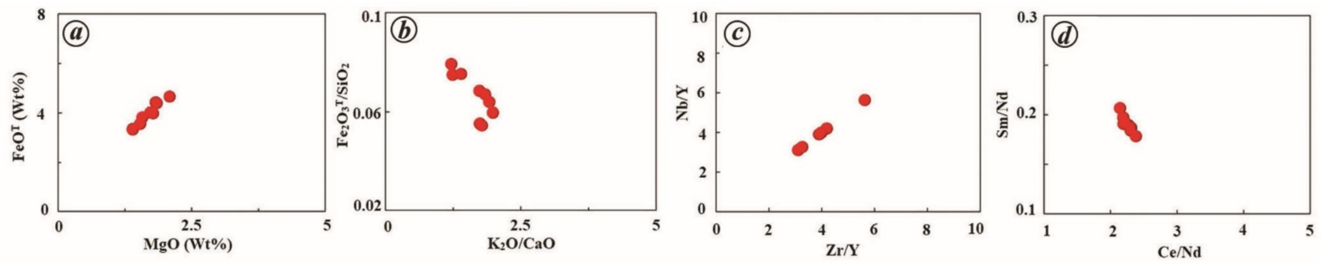

Figure 6. Plots of Kyrdem granitoids showing magma mixing; (***a***) FeO^T versus MgO plot[28]; (***b***) $Fe_2O_3^T/SiO_2$ versus K_2O/CaO; (***c***) Zr/Y versus Nb/Y and (***d***) Ce/Nd versus Sm/Nd plots[29,30].

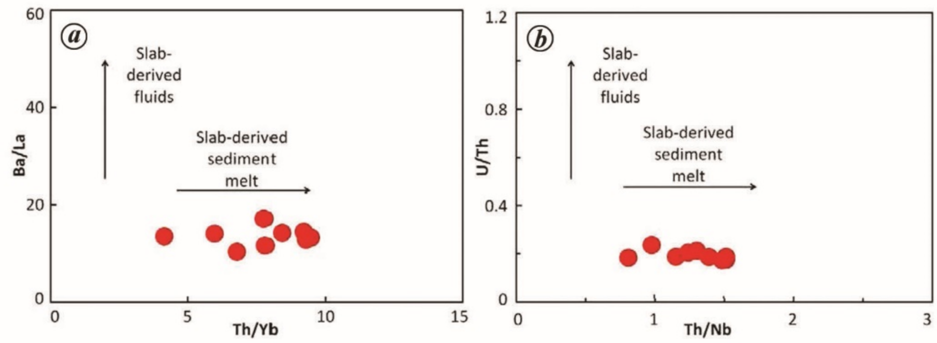

Figure 7. (***a***) Ba/La versus Th/Yb plot[31] and (***b***) U/Th versus Th/Nb plot[19] of Kyrdem granitoids for discriminating the mantle metasomatic source.

bodies. The samples showed typical magma mixing trends in the binary plots involving ratios of major oxides and trace elements like FeO^T versus MgO plot[28], $Fe_2O_3^T/SiO_2$ versus K_2O/CaO, Ce/Nd versus Sm/Nd and Nb/Y versus Zr/Y diagrams[9,29,30] (Figure 6 *a–d*). Shoshonitic granites thus share geochemical features of both crust and mantle sources, and the parent magma was probably formed from mixing both mantle- and crust-derived melts. The elemental pattern in the multi-element diagram and REE plots (Figures 4 *a* and *b*) are typical of subduction-related magmas. The enrichment of LILE and LREE can be explained by partially melting the enriched sub-continental lithospheric mantle, metasomatized by either fluids or sediment-melts from a previously subducted slab. The samples with a higher concentration of Th than U (low U/Th values avg = 0.19) indicate the influence of sediment-derived melts. The high Ba and Sr contents in granitoids also suggest probable mantle metasomatism by subducted sediments (reservoir of Ba, Sr, P, LREEs and Zr). The samples also showed a clear influence of sediment-derived melts in a number of mobile versus immobile trace element ratio plots such as Ba/La versus Th/Yb plot[31] (Figure 7 *a*) and U/Th versus Th/Nb plot[19] (Figure 7 *b*). These plots are used to evaluate the impact of sediment-derived fluids (enrichment in LILEs, e.g. Ba, Sr and Nb) and/or melt derived from sediments (enrichment in LREE and Th) in the metasomatism of the lithospheric mantle.

The low Mg# values (<40) of the studied samples and the SiO_2 versus Mg# plot[32] (Figure 8 *a*) probably suggest that the melts were derived from an amphibolitic (basaltic) source[32]. In the ($Na_2O + K_2O + FeO^T + MgO + TiO_2$) versus ($Na_2O + K_2O$)/($FeO^T + MgO + TiO_2$) plot (Figure 8 *b*) and ($Al_2O_3 + FeO^T + MgO + TiO_2$) versus Al_2O_3/(FeO^T + $MgO + TiO_2$) plot[33] (Figure 8 *c*) with fields of magma derived by partially melting meta-greywackes, metapelites and amphibolites, most of the granitoids occupy the domain of experimental melts from amphibolites with a few samples which occur within the field of amphibolites and/or meta-greywacke source rock. Likewise, in the molar CaO/($MgO + FeO^T$) versus molar Al_2O_3/($MgO + FeO^T$) plot[34] (Figure 8 *d*), the studied granitoids show affinity towards the meta-basaltic source. The strongly metaluminous and slightly peraluminous nature of the granitoids is consistent with the amphibolitic crustal rock as their source, and hence the possibility of their mass derivation from the pelitic source can be discarded[35]. The presence of a thick middle crust beneath the Shillong Plateau has also been reported by several researchers[36]. The SiO_2 versus K_2O and SiO_2 versus Na_2O diagrams with fields of experimental partial melting products of amphibolites[37], metabasalt[32], quartz amphibolites and biotite gneiss[38], and medium- to high-K basaltic rocks[18,35,39,40] are used to constrain the crustal source. In the SiO_2 versus K_2O plot (Figure 8 *e*), the samples occupy the field of melts obtained from medium- to high-K basaltic source rocks. In the SiO_2 versus Na_2O plot, the samples fall within the fields of melt drawn by partially melting amphibolitic and high-alumina bearing medium- to high-K basaltic source rocks that typically belong to

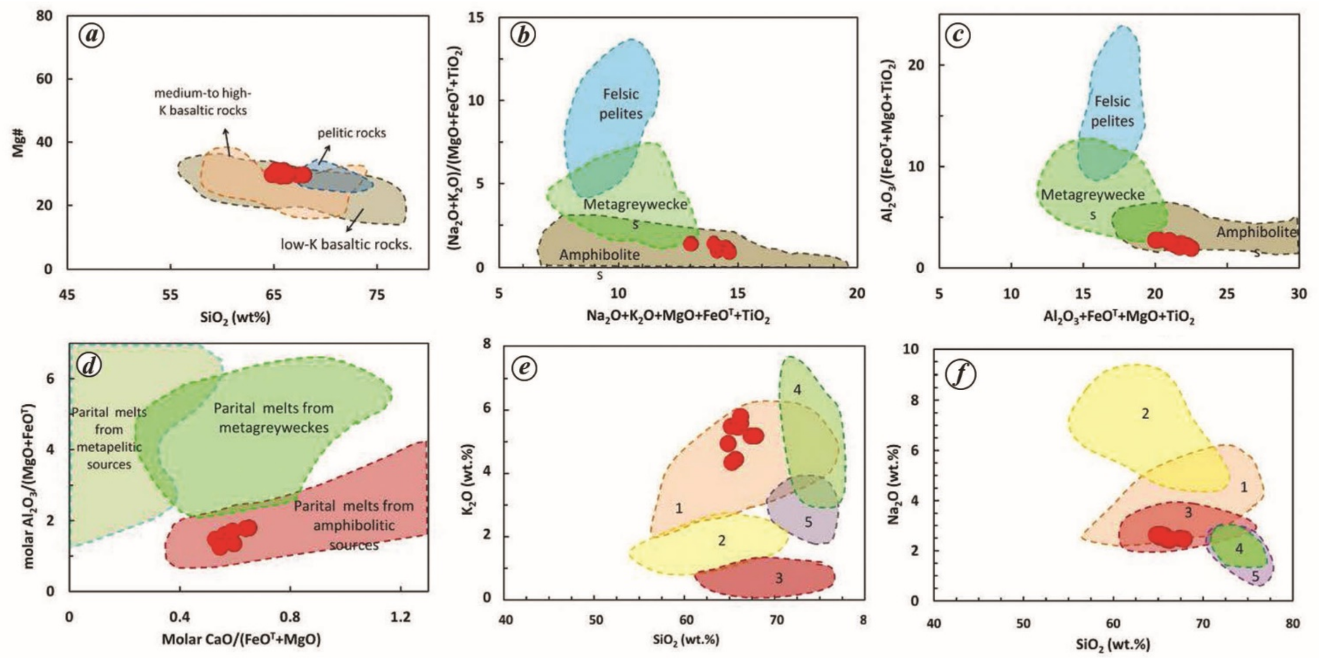

Figure 8. Crustal melt discrimination plots for the Kyrdem granitoids. ***a***, SiO_2 versus Mg# plot[32]; ***b***, $Na_2O + K_2O + FeO^T + MgO + TiO_2$ versus $(Na_2O + K_2O)/(FeO^T + MgO + TiO_2)$; ***c***, $(Al_2O_3 + FeO^T + MgO + TiO_2)$ versus $Al_2O_3/(FeO^T + MgO + TiO_2)$ plot[33]; ***d***, $CaO/(MgO + FeO^T)$ versus $Al_2O_3/(MgO + FeO^T)$ (molar) plot[34]; ***e***, SiO_2 versus K_2O; ***f***, SiO_2 versus Na_2O plots (after Chen *et al.*[40]) with fields for (1) medium- to high-K basaltic rocks[39], (2) metabasalt[32], (3) amphibolites[37], (4) biotite gneiss[38] and (5) quartz amphibolites[38].

subduction tectonic environment[39] (Figure 8 *f*). Thus, a high-K basaltic source emplaced during a previous subduction event and subsequently metamorphosed is considered the crustal source rock for the studied granitoids. Partial melting of metabasaltic middle crust triggered by upwelled enriched lithospheric melt due to slab break-off generated the felsic melt and subsequent mixing of both the melts thus appears as the most probable mechanism for the generation of the shoshonitic granitoids of Shillong plateau in the post-collisional setting.

The study of shoshonitic magmatic rocks provides crucial constraints on probing the nature of the source mantle, tracing magma differentiation processes, tectonic evolution and understanding the metallogenesis of associated mineral deposits. They are closely associated with a variety of mineral deposits, such as the magnetite apatite deposit-related syenitic granite porphyries in Eastern China[41] and porphyry-type copper deposit-related granodiorite porphyries in south-east Iran[42]. They are also found associated with Fe–Cu–Au ore deposits in different parts of the world and thus have attracted wide interest[43,44]. The Kyrdem pluton covers a large area and thus provides scope for the search for potential mineralization and further evaluation within the pluton.

Tectonic setting and geodynamic implications

The Kyrdem shoshonitic granitoids were probably emplaced in a post-collisional setting at ca. 512 Ma (ref. 11), immediately after the final stage of amalgamation of Eastern Gondwana land masses, which culminated at around ca. 500 Ma (refs 10, 11). This suggests that the Shillong Plateau, which was lying on the leading edge of the Indian plate during the collisional phase, has experienced a shift in tectonic regime from compressive to extension setting in a post-collisional environment in the late phase of the orogenic event. Decompression following delamination of the lithospheric root[20] and slab break-off[9] models have been widely proposed to explain the genesis of shoshonitic melt in a post-collisional setting. Since Kyrdem granitoids were emplaced during the last phase of the collisional event as indicated by their isotopic ages, therefore the possibility of lithospheric delamination as a driving mechanism for their genesis may be precluded because a long phase of crustal thickening post-orogeny is necessary for delamination. The slab break-off model, however, may be considered a viable mechanism, as it results in small pockets of felsic magmatism along a suture zone[45], similar to the granitoids of the Shillong Plateau. Chatterjee *et al.*[46] suggested the continuation of the Pan-African suture zone from Prydz Bay of east Antarctica to the Shillong Plateau, along which the Indian plate had amalgamated with the Antarctic and Australian plates at around 500 Ma during the final stage of the Eastern Gondwana assembling. The Kyrdem pluton of the Shillong Plateau might have emplaced during the Cambrian–Ordovician time window along the Pan-African suture zone and thus provides evidence of crustal growth of the plateau during the formation of Eastern Gondwana.

1. Perkins, R. J., Cooper, F. J., Condon, D. J., Tattitch, B. and Naden, J., Post-collisional Cenozoic extension in the northern Aegean: the high-K to shoshonitic intrusive rocks of the Maronia Magmatic Corridor, northeastern Greece. *Lithosphere*, 2018, **10**, 582–601.
2. Rezeau, H., Leuthold, J., Tayan, R., Hovakimyan, S., Ulianov, A., Kouzmanov, K. and Moritz, R., Incremental growth of mid- to upper-crustal magma bodies during Arabia–Eurasia convergence and collision: a petrological study of the calc-alkaline to shoshonitic Meghri-Ordubad pluton (southern Armenia and Nakhitchevan, Lesser Caucasus). *J. Petrol*., 2018, **59**, 931–966.
3. Ding, L. X., Ma, C. Q., Li, J. W., Robinson, P. T., Deng, X. D., Zhang, C. and Xu, W. C., Timing and genesis of the adakitic and shoshonitic intrusions in the Laoniushan complex, southern margin of the North China Craton: implications for post-collisional magmatism associated with the Qinling Orogen. *Lithos*, 2011, **126**, 212–232.
4. Beccaluva, L., Bianchini, G., Mameli, P. and Natali, C., Miocene shoshonite volcanism in Sardinia: implications for magma sources and geodynamic evolution of the central western Mediterranean. *Lithos*, 2013, **180**, 128–137.
5. Liu, X., Liu, W. and Si, C., Petrogenesis and source rocks of the high-K calc-alkaline and shoshonitic I-type granitoids in the northwestern part of East Junggar, NW China. *Lithos*, 2019, **326**, 298–312.
6. Manley, C. R., Glazner, A. F. and Farmer, G. L., Timing of volcanism in the Sierra Nevada of California: evidence for Pliocene delamination of the batholithic root? *Geology*, 2000, **28**, 811–814.
7. Bloomer, S. H., Stern, R. J., Fisk, E. and Geschwind, C. H., Shoshonitic-volcanism in the Northern Mariana arc: mineralogic and major and trace element characterisitics. *J. Geophys. Res*., 1989, **94**, 4469–4496.
8. Xu, C., He, Y. K., Zheng, R. G., Zhang, W., Meng, Q. P. and Zhang, Y. Y., Geochemical characteristics of Early Cretaceous shoshonites in the middle and western northern margin of the North China Craton and a comparative study. *Acta Sci. Nat. Univ. Pekinensis*, 2014, **50**, 301–315 (in Chinese with English abstract).
9. Goswami, B. and Bhattacharyya, C., Petrogenesis of shoshonitic granitoids, eastern India: implications for the late Grenvillian post-collisional magmatism. *Geosci. Front*., 2014, **5**, 821–843.
10. Chatterjee, N., Constraints from monazite and xenotime growth modelling in the MnCKFMASH-PYCe system on the P–T path of a metapelites from Shillong–Meghalaya Plateau: implications for the Indian shield assembly. *J. Metamorph. Geol*., 2017, **35**, 393–412.
11. Kumar, S., Rino, V., Hayasaka, Y., Kimura, K., Raju, S., Terada, K. and Pathak, M., Contribution of Columbia and Gondwana Supercontinent assembly- and growth-related magmatism in the evolution of the Meghalaya Plateau and the Mikir Hills, Northeast India: constraints from U–Pb SHRIMP zircon geochronology and geochemistry. *Lithos*, 2017, **277**, 356–375.
12. Ghatak, A. and Basu, A. R., Remnants of the Kerguelen plume in eastern India: evidence from Nd–Sr–Pb isotopic and trace element geochemistry of Sylhet Traps, Shillong Plateau. *Am. Geophys. Union*, 2006, **87**, 52.
13. Ghatak, A. and Basu, A. R., Isotopic and trace element geochemistry of alkalic–mafic–ultramafic–carbonatitic complexes and flood basalts in NE India: origin in a heterogeneous Kerguelen plume. *Geochim. Cosmochim. Acta*, 2013, **115**, 46–72.
14. Kumar, G. R. R. and Sreejith, C., Petrology and geochemistry of charnockites (felsic ortho-granulites) from the Kerala Khondalite Belt, southern India: evidence for intra-crustal melting, magmatic differentiation and episodic crustal growth. *Lithos*, 2016, **262**, 334–354.
15. Feng, W. and Zhu, Y., Petrogenesis and tectonic implications of the late Carboniferous calc- alkaline and shoshonitic magmatic rocks in the Awulale mountain, western Tianshan. *Gondwana Res*., 2019, **76**, 44–61.
16. Morrison, G. W., Characteristics and tectonic setting of the shoshonite rock association. *Lithos*, 1980, **13**, 97–108.
17. Turner, S. *et al.*, Post-collision shoshonitic volcanism on the Tibetan Plateau: implications for convective thinning of the lithosphere and the source of ocean island basalts. *J. Petrol*., 1996, **37**, 45–71.
18. Jiang, Y. H., Jia, R. Y., Liu, Z., Liao, S. Y., Zhao, P. and Xhou, Q., Origin of Middle Triassic high-K calc-alkaline granitoids and their potassic microgranular enclaves from the western Kunlun orogeny, northwest China: a record of the closure of Paleo-Tethys. *Lithos*, 2013, **156–159**, 13–30.
19. Karsli, O., Dokuz, A., Uysal, I., Ketenci, M., Chen, B. and Kandemir, R., Deciphering the shoshonitic monzonites with I-type characteristic, the Sisdagi pluton, NE Turkey: magmatic response to continental lithospheric thinning. *J. Asian Earth Sci*., 2012, **51**, 45–62.
20. Jia, L., Wang, L., Wang, G., Lei, S. and Wu, X., Petrogenesis of the Late Triassic shoshonitic Shadegai pluton from the northern North China Craton: implications for crust–mantle interaction and post-collisional extension. *Geosci. Front*., 2019, **10**, 595–610.
21. Müller, D. and Forresta, I. P., The shoshonite porphyry Cu–Au association at Bajo de la Alumbrera, Catamarca Province, Argentina. *Mineral. Petrol*., 1998, **64**, 47–64.
22. Sun, S. S. and McDonough, W. F., Chemical and isotopic systematics of oceanic basalts: implications for mantle composition and processes. In *Magmatism in Ocean Basins* (eds Saunders, A. D. and Norry, M. J.), Geological Society, London, Special Publications, 1989, vol. 42, pp. 313–345.
23. Jiang, Y. H., Jiang, S. Y., Ling, H. F., Zhou, X. R., Rui, X. J. and Yang, W. Z., Petrology and geochemistry of shoshonitic plutons from the western Kunlun orogenic belt, northwestern Xinjiang, China: implications for granitoid geneses. *Lithos*, 2002, **63**, 165–187.
24. Müller, D., Rock, N. M. S. and Groves, D. I., Geochemical discrimination between shoshonitic and potassic volcanic rocks in different tectonic settings: a pilot study. *Mineral. Petrol*., 1992, **46**, 259–289.
25. De la Roche, H., Leterrier, J., Grand-Claude, P. and Marchal, M., A classification of volcanic and plutonic rocks using R1R2-diagram and major element analyses – its relationship with current nomenclature. *Chem. Geol*., 1980, **29**, 183–210.
26. Batchelor, A. R. and Bowden, P., Petrogenetic interpretation of granitoid rock series using multicationic parameter. *Chem. Geol*., 1985, **48**, 43–55.
27. Zhao, Q., Xiao, R., Zhang, D., Wang, J., Zhang, Y. and Li, P., Petrogenesis and tectonic setting of ore-associated intrusive rocks in the Baiyinnuoer Zn–Pb deposit, southern Great Xing'an Range (NE China): constraints from zircon U–Pb dating, geochemistry, and Sr–Nd–Pb isotopes. *Minerals*, 2020, **10**, 19; doi:10.3390/min10010019.
28. Zorpi, M. J., Coulon, C., Orsini, J. B. and Cocirta, C., Magma mingling, zoning and emplacement in calc-alkaline granitoid plutons. *Tectonophysics*, 1989, **157**, 315–329.
29. Zhou, X. R., Hybridization in the genesis of granitoids. *Front. Earth Sci*., 1994, **1**, 77–97.
30. Neves, S. P. and Vauchez, A., Successive mixing and mingling of magmas in a plutonic complex of Northeast Brazil. *Lithos*, 1995, **34**, 275–299.
31. Woodhead, J. D., Hergt, J. M., Davidson, J. P. and Eggins, S. M., Hafnium isotope evidence for 'conservative' element mobility during subduction zone processes. *Earth Planet. Sci. Lett*., 2001, **192**, 331–346.
32. Rapp, P. R. and Watson, E. B., Dehydration melting of metabasalt at 8–32 Kbar: implications for continental growth and crust–mantle recycling. *J. Petrol*., 1995, **36**, 891–931.
33. Patiño Douce, A. E., What do experiments tell us about the relative contributions of crust and mantle to the origin of granitic magmas. In *Understanding Granites: Integrating New and Classical Techniques* (eds Castro, A., Fernández, C. and Vigneresse, J. L.), Geol. Soc. Lon. Spec. Pub., 1999, vol. 168, pp. 55–75.
34. Altherr, F. F., Holl, A., Hegner, E., Langer, C. and Kreuzer, H., High-potassium, calc-alkaline I-type plutonism in the European variscides: northern Vosges (France) and northern Schwarzwald (Germany). *Lithos*, 2000, **50**, 51–73.

35. Roy, P., Goswami, B., Dutta, S. and Bhattacharyya, C., Petrogenesis of the post-collisional porphyritic granitoids from Jhalida, Chhotanagpur Gneissic Complex, eastern India. *Geol. Mag.*, 2021, **158**, 598–634.
36. Borah, K., Bora, D. K., Goyal, A. and Kumar, R., Crustal structure beneath northeast India inferred from receiver function modeling. *Phys. Earth Planet. Int.*, 2016, **258**, 15–27.
37. Beard, J. S. and Lofgren, G. E., Dehydration melting and water-saturated melting of basaltic and andesitic greenstones and amphibolites at 1, 3, and 6. 9 kb. *J. Petrol.*, 1991, **32**, 365–401
38. Patiño Douce, A. E. and Beard, J. S., Dehydration–melting of biotite gneiss and quartz amphibolite from 3 to 15 kbar. *J. Petrol.*, 1995, **36**, 707–38.
39. Sisson, T. W., Ratajeski, K., Hankins, W. B. and Glazner, A. F., Voluminous granitic magmas from common basaltic sources. *Contrib. Mineral. Petrol.*, 2005, **148**, 635–661.
40. Chen, J., Yang, J. H., Zhang, J. H., Sun, J. F. and Wilde, S. A., Petrogenesis of the Cretaceous Zhangzhou batholith in southeastern China: zircon U–Pb age and Sr–Nd–Hf–O isotopic evidence. *Lithos*, 2013, **162–163**, 140–156.
41. Mao, J. W., Xie, G. Q., Duan, C., Pirajno, F., Ishiyama, D. and Chen, Y. C., A tectono-genetic model for porphyry-skarn-stratabound Cu–Au–Mo–Fe and magnetite–apatite deposits along the middle–lower Yangtze River Valley, Eastern China. *Ore Geol. Rev.*, 2011, **43**, 294–314.
42. Hosseini, M., Ghaderi, R., Alirezaei, S. and Sun, W. D., Geological characteristics and geochronology of the Takht-e-Gonbad copper deposit, SE Iran: a variant of porphyry type deposits. *Ore Geol. Rev.*, 2017, **86**, 440–458.
43. Zhu, Y. F., An, F., Feng, W. Y. and Zhang, H. C., Geological evolution and huge ore-forming belts in the core part of the central Asian metallogenic region. *J. Earth Sci.*, 2016, **27**, 491–506.
44. Zhao, X. B., Xue, C. J., Chi, G. X., Zhao, Y. and Yan, Y. H., Diabase-hosted copper mineralization in the Qunjsai deposit, west Tianshan, NW China: geological, geochemical and geochronological characteristics and mineralization mechanism. *Ore Geol. Rev.*, 2018, **92**, 430–448.
45. Atherton, M. P. and Ghani, A. A., Slab breakoff: a model for Caledonian, late granite syncollisional magmatism in the orthotectonic (metamorphic) zone of Scotland and Donegal, Ireland. *Lithos*, 2002, **62**, 65–85.
46. Chatterjee, N., Mazumdar, A. C., Bhattacharya, A. and Saikia, R. R., Mesoproterozoic granulites of the Shillong–Meghalaya Plateau: evidence of westward continuation of the Prydz Bay Pan-African suture into Northeastern India. *Precambrian Res.*, 2007, **152**, 1–26.
47. Srivastava, R. K. and Sinha, A. K., Geochemistry of early cretaceous alkaline ultramafic–mafic complex from Jasra, Karbi Anglong, Shillong Plateau, Northeastern India. *Gondwana Res.*, 2004, **7**, 549–561.
48. Kumar, S. and Singh, K. M., Granite series evaluation of Early Ordovician Kyrdem granitoids and enclaves, Meghalaya plateau, northeast India: implication on oxidation condition of interacting mafic–felsic magma system. *Earth Sci. India*, 2008, **1**, 204–219.
49. Singh, M. S., Geochemical and petrogenetic studies of the porphyritic granitoids of Kyllang–Moudoh pluton of Shillong Plateau, Meghalaya. Doctoral thesis, University of Delhi, 2013.
50. Ghosh, S., Chakraborty, S., Paul. D. K., Bhalla, J. K., Bishui, P. K. and Gupta, S. N., New Rb–Sr isotopic ages and geochemistry of granitoids from Meghalaya and their significance in middle to late Proterozoic crustal evolution. *Indian Mineral*, 1994, **48**, 33–44.
51. O'Connor, J. T., A classification of quartz-rich igneous rocks based on feldspar ratios. United State Geological Survey, Denver, Colorado, 1965, pp. 79–84.
52. Baker, M. B., Hirschmann, M. M., Ghiorso, M. S. and Stolper, E. M., Compositions of near-solidus peridotite melts from experiments and thermodynamic calculations. *Nature*, 1995, **375**, 308–311.
53. Frost, B. R., Barnes, C. G., Collins, W. J., Arculus, R. J., Ellis, D. J. and Frost, C. D., A geochemical classification for granitic rocks. *J. Petrol.*, 2001, **42**, 2033–2048.
54. Peccerillo, A. and Taylor, S. R., Geochemistry of Eocene calc-alkaline volcanic rocks from the Kastamonu area, northern Turkey. *Contrib. Mineral. Petrol.*, 1976, **58**, 63–81.
55. Pearce, J. A., Trace element characteristics of lavas from destructive plate margins. In *Andesites* (ed. Thorp, R. S.), John Wiley, New York, USA, 1982, pp. 525–548.

ACKNOWLEDGEMENTS. We thank the Head, Department of Earth Science, Assam University, Silchar, for providing the necessary laboratory facilities to carry out this work. We also thank the Directors of CSIR-NGRI and NCESS, Thiruvananthapuram, for geochemical analysis. This research is financially supported by the Department of Science and Technology, Government of India under the Inspire Research Fellowship Programme (File No.: DST/Inspire Fellowship/2016/IF160812) awarded to D.C. Constructive comments by Prof. Talat Ahmad (Wadia Institute of Himalayan Geology, Dehradun) and an anonymous reviewer, and efficient editorial handling by Prof. Somnath Dasgupta are acknowledged.

Received 28 February 2023; revised accepted 7 June 2023

doi: 10.18520/cs/v125/i6/655-664